PHYSICAL REVIEW C VOLUME 22, NUMBER 1 JULY 1980

Angular distributions in a unified model of preequilibrium and equilibrium neutron emission

J. M. Akkermans* and H. Gruppelaar
Netherlands Energy Research Foundation (ECN), Petten (N.H.), The Netherlands

G. Reffo
Centro di Recerche E. Clementel, Comitato Nazionale Energia Nucleare, Via Mazzini 2, Bologna, Italy
(Received 19 November 1979)

An alternative mathematical formulation is presented for the generalized master equation of the exciton model, introduced by Mantzouranis *et al.* to describe preequilibrium effects in angular distributions of emitted particles in nuclear reactions. The exciton model proposed in this paper includes internal transitions with $\Delta n = 2, 0, -2$, and describes both the preequilibrium and the equilibrium stages of the reaction process. A simple, but exact formula is given to calculate mean lifetimes of exciton states and their Legendre coefficients, from which double differential cross sections can be easily calculated. The mathematical improvements of the generalized exciton model greatly facilitate a systematical comparison with experimental data. In this paper the neutron inelastic scattering data for 34 elements measured by Hermsdorf *et al.* at 14.6 MeV were used for such intercomparison. The results show underestimation of angular distributions at backward angles. However, a good overall fit of all angular distributions is obtained by adjustment of only two global parameters. It is concluded that further study with regard to the physics of the model is required. Some local variations in the angular distribution coefficients as a function of the mass number might be ascribed to level-density effects. Although it appeared that the presently adopted formulas and parameters in exciton model calculations are not adequate to give detailed predictions of the energy and angular distributions, meaningful improvements were obtained by variation of final-state parameters. Finally, some attention was devoted to the unification of the exciton and Hauser-Feshbach models. By introducing a proper definition of "equilibrium" emission it is shown that consistent results are obtained for neutron emission spectra calculated with the two models.

[NUCLEAR REACTIONS Be, C, Na, Mg, Al, Si, P, S, Ca, Ti, V, Cr, Mn, Fe, Co, Ni, Cu, Zn, Ga, Se, Br, Zr, Nb, Cd, In, Sn, Sb, I, Ta, W, Au, Hg, Pb, Bi (n,nx), $E=14.6$ MeV; calculated $\sigma(E_n,\theta)$, Legendre coefficients. Generalized exciton model, preequilibrium and equilibrium analysis, Hauser-Feshbach model.]

I. INTRODUCTION

Preequilibrium statistical theory has proved to be very useful for calculating spectra of light particles emitted in nuclear reactions at energies ranging from 10 up to about 100 MeV. An important problem in preequilibrium theory is how to describe the angular distributions of emitted particles. In this paper we will discuss this problem in the framework of the exciton model. Several improvements of the theory are proposed. Comparison is made with experimental data of inelastic neutron scattering at 14.6 MeV for a set of 34 nuclides, a choice motivated by our interest in possible applications of this work, e.g., in the field of design calculations for future fusion reactors. Some theoretical results presented here have already been published in a short communication.[1]

For the analysis of preequilibrium angular distributions, Mantzouranis *et al.*[2,3] have proposed a generalization of the master-equation exciton model for fast nucleons as incoming particles. In this model, the state of the composite nucleus is thought to be characterized at each time t by the exciton number n and a direction Ω, which corresponds to the direction of the projectile on its way inside the nucleus. In a series of binary collisions with the target nucleons, the projectile gradually loses its energy as well as its correlation with the incident, forward direction. It is assumed that, when emission occurs from a nucleus in state (n, Ω), the direction of the emitted particle coincides with Ω. Thus, the first few collisions (also corresponding to the lowest exciton numbers) generate the forward peaking in the emission cross sections, which distinguishes the preequilibrium part from the evaporative part of the reaction.

The above-mentioned authors factorize the generalized internal transition rates from state (n, Ω) to state (m, Ω') into the usual transition rates between different exciton states and an angle-dependent part that is supposed to be proportional to the differential free nucleon-nucleon scattering cross section:

$$\lambda_{n\to m}(\Omega\to\Omega') = \lambda_{n\to m} G(\Omega,\Omega') = \lambda_{n\to m}\left(\int d\Omega\,\frac{d\sigma^f}{d\Omega}\right)^{-1}\frac{d\sigma^f}{d\Omega}\,. \tag{1}$$

Let $q(n,\Omega,t)$ denote the occupation probability for the composite nucleus state (n,Ω) at time t. The generalized master equation then reads

$$\frac{d}{dt}q(n,\Omega,t) = \sum_{m=n-2}^{n+2}\lambda_{m\to n}\int d\Omega' G(\Omega,\Omega')q(m,\Omega',t) - q(n,\Omega,t)\left(w(n)+\sum_{m=n-2}^{n+2}\lambda_{n\to m}\right), \tag{2}$$

where we have included an emission term with emission rate $w(n)$. The positive terms at the right-hand side of Eq. (2) describe the feeding to state (n,Ω) from all possible states (m,Ω'), whereas the negative terms account for the losses of the system due to emission and to transitions to other exciton states.

Strictly speaking, transitions with $\Delta n = 0$ have to be included in the generalized master equation. In contrast to the angle-integrated case, these λ^0 terms may not be dropped from the equation because of the fact that each collision contributes to the loss of correlation with the initial direction, irrespective of whether the exciton number has been changed after the collision or not. Carrying out a solid-angle integration in Eq. (2), the $\Delta n = 0$ terms cancel and the well-known angle-integrated master equation is left[4]:

$$\frac{d}{dt}q(n,t) = \lambda^+(n-2)q(n-2,t) + \lambda^-(n+2)q(n+2,t) - q(n,t)[w(n)+\lambda^+(n)+\lambda^-(n)], \tag{3}$$

where $\lambda^\pm(n) = \lambda_{n\to n\pm 2}$.

Comparing Eqs. (2) and (3), it is obvious that the solid-angle integrals in Eq. (2) spoil the simple mathematical structure of the master equation (3). Mantzouranis *et al.* have solved the generalized master equation by numerical methods. However, these methods are very time consuming. Moreover, the calculations of spectra and of angular distributions have to be performed in completely different ways. In this paper it is shown that it is possible to reduce the generalized master equation to a form similar to that of the standard master equation (3). This reduction offers a very fast and simple method to calculate both nucleon spectra and angular distributions, without needing to introduce approximations.

In Sec. II this quite general formalism for the solution of the generalized master equation is discussed. An important aspect of the model is that both equilibrium and preequilibrium components are treated in a consistent way. The relation with previously introduced closed-form expressions is also shortly discussed. Section III specifies the model parameters, which have been adopted to calculate the angular distributions.

The above-mentioned mathematical improvements of the model facilitate a systematical intercomparison of experimental and calculated data for a large class of experiments, such as those performed by Hermsdorf *et al.*[5] for neutron-induced emission spectra at 14.6 MeV. The results of this comparison for neutron emission spectra and angular distributions are discussed in Sec. IV. In this discussion the role of level densities in calculations with preequilibrium models is emphasized. The relation with conventional statistical-model calculations is also indicated. For this purpose, rather sophisticated calculations have been performed with a recently developed code.[6] Finally, in Sec. V some conclusions and recommendations for further development of the theory are given.

II. GENERAL THEORY OF THE GENERALIZED EXCITON MODEL

A. Diagonalization of the integral operator

In order to reduce the generalized master equation (2), let us investigate the eigenfunctions of the integral operator V defined by

$$Vf(\Omega) = \int d\Omega' G(\Omega,\Omega')f(\Omega')\,, \tag{4}$$

where f is any quadratically integrable function on the surface of the unit ball, and the kernel G is given by Eq. (1).

As a consequence of Eq. (1), the integral kernel G only depends on the angle α between the ingoing and outgoing directions Ω and Ω'. Hence it is possible to expand the kernel G into a Legendre polynomial series. The addition theorem for spherical harmonics then leads to the conclusion that the spherical harmonics form a complete set of eigenfunctions of the integral operator V. In Ref. 1 this result was obtained by applying Schur's lemma.

Due to the axial symmetry of the solutions $q(n,\Omega,t)$ of Eq. (2) with respect to the incident direction of the projectile (cf. Ref. 3, Appendix A), we only have to deal with those eigenfunctions of V that are independent of the azimuthal angle ϕ, i.e., the Legendre polynomials P_l. Therefore, the integral operator occurring in the generalized master equation can be diagonalized according to

$$\int d\Omega' G(\Omega,\Omega')P_l(\cos\theta') = \mu_l P_l(\cos\theta)\,, \tag{5}$$

where μ_l is the eigenvalue of V corresponding to

the Legendre polynomial of order l.

The eigenvalues can be determined as follows. Choosing $\theta = 0$ in Eq. (5), we may define $\int_0^{2\pi} G(\Omega, \Omega')d\phi' = h(x)$, where $x = \cos\alpha$. In general, then, the eigenvalues μ_l are simply given by

$$\mu_l = \int_{-1}^{+1} h(x)P_l(x)dx . \tag{6}$$

The evaluation of these integrals will be discussed in more detail in Sec. III.

Next, we expand the generalized occupation probability $q(n, \Omega, t)$ into a Legendre polynomial series:

$$q(n, \Omega, t) = \sum_l \eta_l(n, t)P_l(\cos\theta) . \tag{7}$$

Making use of Eqs. (5) and (7), taking advantage of the orthogonality of the Legendre polynomials, the generalized master equation reduces to the following set of equations:

$$\begin{aligned}\frac{d}{dt}\eta_l(n, t) = {} & \mu_l\lambda^+(n-2)\eta_l(n-2, t) \\ & + \mu_l\lambda^-(n+2)\eta_l(n+2, t) \\ & - \eta_l(n, t)[w(n) + \lambda^+(n) + \lambda^-(n) \\ & + (1-\mu_l)\lambda^0(n)] .\end{aligned} \tag{8}$$

Thus, the integro-differential equation (2) has been transformed to a set of linear differential equations, one for each Legendre polynomial of order l. The form of these new master equations for the Legendre coefficients of $q(n, \Omega, t)$ is identical with that of the angle-integrated master equation (3). Consequently, the calculation of preequilibrium angular distributions and the determination of preequilibrium spectra can be performed along exactly the same lines. In particular, the same routines in a computer code can be used.

B. Solution of the generalized master equation

Let us write Eq. (8) in matrix form

$$\frac{d}{dt}\underline{\eta}_l(t) = \underline{B}_l\underline{\eta}_l(t) . \tag{9}$$

Here, $\underline{B}_l$ symbolizes the matrix of the transition rates. Equation (8) shows that we are dealing with a tridiagonal matrix, a consequence of the postulated two-body nature of the intranuclear collisions.

Since $\int d\Omega' G(\Omega, \Omega') = 1$ according to Eq. (1), it is immediately seen from Eq. (6) that $\mu_0 = 1$ and $|\mu_l| < 1$ for $l \geq 1$. It may be noted therefore that for $l = 0$, the λ^0 transitions cancel and that B_0 is identical with the transition rate matrix of the angle-integrated master equation (3).

With the aid of standard matrix-algebraic theorems it is easily demonstrated that the transition matrix $\underline{B}_l$ can be diagonalized, and that all its eigenvalues are real and negative.[7] Luider[8] already proved this for the angle-integrated master equation. Hence, the analytical, time-dependent solution of the generalized master equation is

$$\underline{\eta}_l(t) = \sum_i (c_l)_i(\underline{y}_l)_i \exp[(\nu_l)_i t] , \tag{10}$$

where $(\underline{y}_l)_i$ and $(\nu_l)_i$ denote the eigenvectors and eigenvalues of $\underline{B}_l$, respectively, and $(c_l)_i$ are integration constants to be determined from the initial condition.

Next, let us denote by ρ the maximum eigenvalue of $\underline{B}_0$ (i.e., the eigenvalue with the smallest absolute value). Then it may be inferred from the Perron-Frobenius theorem and a lemma due to Wielandt (see, e.g., Ref. 9) that

$$\nu_l < \rho \quad (l \geq 1) \tag{11}$$

for all eigenvalues ν_l of $\underline{B}_l$. Accordingly, after a long lapse of time, the $l = 0$ term in Eq. (10) with eigenvalue ρ will dominate. This formally proves that the angular distributions as predicted by the generalized master equation will become isotropic in the limit $t \to \infty$. This agrees with the intuitive picture that the forward peaking in the angular distributions should be produced in the first stages of the reaction, whereas the evaporational part which corresponds to emission at later times should be roughly isotropic. Figure 1 illustrates this effect for the case of ^{93}Nb. Here, the time evolution of the neutron emission cross section $(d\sigma/d\Omega)(n, n')$ is shown by integrating Eq. (10) from $t = 0$ up to a given time T.

C. Time integral over the solution

In direct generalization of the standard exciton model, the double differential cross section can be computed from

$$\frac{d^2\sigma}{d\epsilon d\Omega}(a, b) = \sigma_a \sum_n w_b(n, \epsilon)\tau(n, \Omega) , \tag{12}$$

where $\tau(n, \Omega) = \int_0^\infty q(n, \Omega, t)dt$, σ_a is the composite nucleus formation cross section, and $w_b(n, \epsilon)$ denotes the average emission rate of particle b with energy ϵ from exciton state n. The summation in Eq. (12) extends over all possible exciton numbers n, thus yielding both the preequilibrium and the equilibrium contributions to the cross section.

With regard to applications, therefore, we are mainly interested in the total time integral of the generalized occupation probability. The preceding results enable us to directly calculate this time integral $\tau(n, \Omega)$. For that purpose $\tau(n, \Omega)$ is also

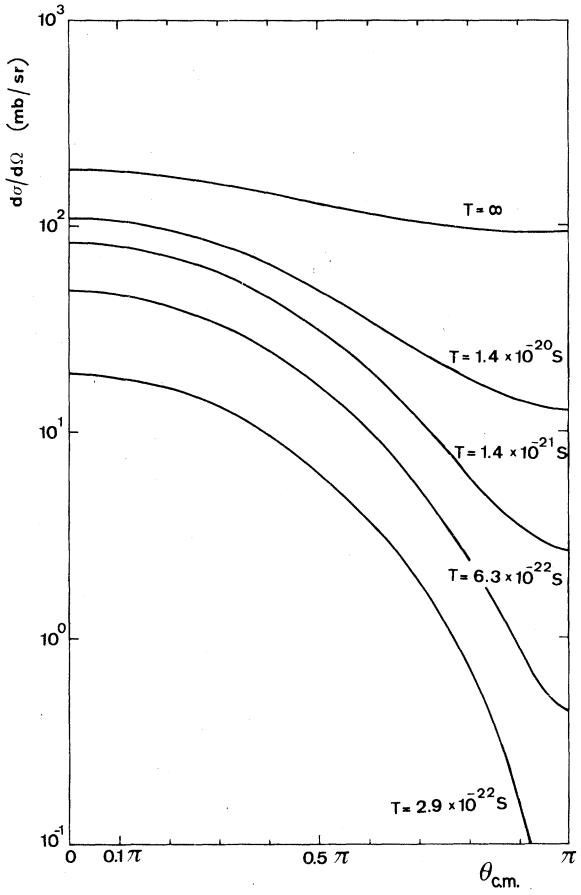

FIG. 1. Time evolution of neutron emission cross section $(d\sigma/d\Omega)(n,n')$ for ^{93}Nb at $E=14.6$ MeV. No secondary neutron emission has been taken into account.

expanded into a Legendre series:

$$\tau(n,\Omega)=\sum_l \zeta_l(n)P_l(\cos\theta)\,. \tag{13}$$

Owing to the fact that all eigenvalues of $\underline{B}_l$ are real and negative, time integration of Eq. (9) from $t=0$ up to infinity immediately yields

$$-\underline{\eta}_l(t=0)=\underline{B}_l\underline{\zeta}_l\,. \tag{14}$$

Here, the left-hand side contains the Legendre coefficients of the initial condition, to be further discussed in Sec. III. Equation (14) uniquely determines the total time integral $\tau(n,\Omega)$.

Instead of solving the generalized master equation (2) numerically and computing the time integral of the solution iteratively, Eqs. (13) and (14) show that the same can be accomplished in a much more convenient way by solving a set of simple tridiagonal matrix equations. A special feature of our formulation is that it directly gives the Legendre expansion coefficients of the angular distributions.

Figure 2 shows the angular dependence of the

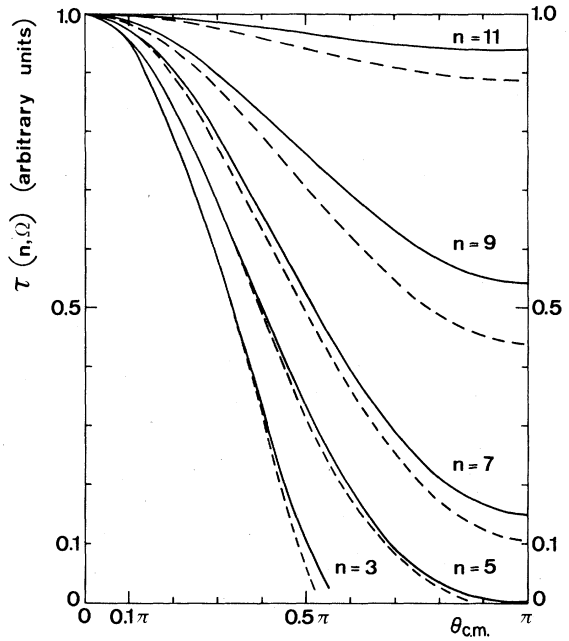

FIG. 2. Angular dependence of mean lifetime $\tau\,(n,\Omega)$ for different values of n. The values $\tau\,(n,\Omega)$ have been normalized to 1 at $\theta_{\text{c.m.}}=0$. Calculations have been performed for ^{93}Nb+n at $E=14.6$ MeV. The solid lines represent the results of a calculation with the full generalized master equation; the dashed lines are calculated with $\lambda^0=0$. Here, $n_0=3$.

quantities $\tau(n,\Omega)$ determined according to Eq. (14) for different exciton numbers. The solid lines represent values of $\tau(n,\Omega)$, normalized to unity at $\theta=0$ and calculated for ^{93}Nb+n at an incident neutron energy of 14.6 MeV. These curves give an impression of the loss of correlation with incident direction, when the exciton number n increases (i.e., when the number of intranuclear collisions that has taken place increases). The dashed lines in Fig. 2 represent the same quantities calculated by neglecting λ^0 transitions. It is clearly demonstrated that λ^0 transitions contribute to a more rapid convergence to isotropy, as pointed out in the Introduction.

D. Closed-form expressions for the angular distributions

According to the generalized exciton model, the forward peaking associated with preequilibrium angular distributions will be produced by emission from the most simple particle-hole configurations, i.e., the states with low exciton numbers In these lowest exciton states the transitions with exciton-number change $\Delta n=+2$ are overwhelmingly more probable than those with $\Delta n=0$ or $\Delta n=-2$. Therefore, it should be possible to obtain good approximations to the exact solution of the generalized master equation by neglecting λ^- or λ^0

transitions. This simplification is often also introduced in the angle-integrated exciton model (and the hybrid model), to obtain simple approximative closed-form expressions.

First, let us drop from the generalized master equation the λ^- transitions only. Then, we may write the solution for the Legendre coefficients $\zeta_l(n)$ of the time integral $\tau(n,\Omega)$ at once by applying Cramer's rule to Eq. (14):

$$\zeta_l(n)=\frac{\eta_l(n_0,t=0)(\mu_l)^{(n-n_0)/2}}{\lambda^+(n)+w(n)+(1-\mu_l)\lambda^0(n)} \times \prod_{\substack{m=n_0\\ \Delta m=2}}^{n-2}\left(\frac{\lambda^+(m)}{\lambda^+(m)+w(m)+(1-\mu_l)\lambda^0(m)}\right), \tag{15}$$

where we have assumed, as usually done, that the system starts in the minimum exciton number n_0. This approximative solution of the generalized master equation demonstrates the role of $\Delta n=0$ transitions. They contribute in a different way to different Legendre orders l, the weight factors being related to the eigenvalues of the integral operator in the generalized master equation.

Another, more simple, closed-form expression can be obtained by neglecting both $\Delta n=0$ and $\Delta n=-2$ transitions. Dropping the λ^0 terms in Eq. (15) it is seen that

$$\zeta_l(n)=\frac{\eta_l(n_0,t=0)(\mu_l)^{(n-n_0)/2}}{\lambda^+(n)+w(n)}D_n, \tag{16}$$

where D_n denotes the commonly used depletion factor in the angle-integrated exciton model.[10] Consequently, here we have

$$\tau(n,\Omega)=\tau(n)\sum_l(\mu_l)^{(n-n_0)/2} \times \eta_l(n_0,t=0)P_l(\cos\theta)\quad(n<\bar{n}), \tag{17}$$

$\tau(n)$ being the mean lifetime of an n-exciton state as given by the usual closed-form exciton model, and $\bar{n}$ the "equilibrium" exciton number. For the calculation of cross sections one could add a Hauser-Feshbach contribution to account for the equilibrium part of the reaction. It has been pointed out previously[1] that a formula similar to Eq. (17) may be written for the hybrid model. Likewise, this formula might be extended to the geometry-dependent hybrid model (for a review of these models see Ref. 11).

Expression (17) very clearly reveals some physical aspects of the preequilibrium reaction process. Neglecting λ^0 and λ^- transitions, as was done in deriving Eq. (17), it takes precisely $(n-n_0)/2$ collisions to create the nth exciton state. The zeroth-order eigenvalue μ_0 describes the isotropic part of the angular distribution. This eigenvalue being equal to one, the higher-order eigenvalues are a measure for the relative contributions of the nonisotropic parts to the angular distribution. These anisotropic contributions decrease according to the number of collisions that has taken place in forming the nth exciton state. This means that the eigenvalues μ_l together with the number of collisions in the nth exciton state quantitatively describe the dissipation of correlation with the incident direction. Thus, this closed-form expression quite explicitly clarifies the general physical picture underlying the generalized master equation.

Figure 3, which has to be compared with Fig. 2, shows the angular dependence of $\tau(n,\Omega)$ according to Eq. (17) for different exciton numbers. It is seen that the development towards istropy proceeds much less rapidly than when the generalized master equation is solved. This would lead to a more forward-peaked angular distribution.

Recently, a method was proposed by Akkermans[12] to obtain the solution of the standard time-integrated master equation in closed form without introducing any simplification. Now that we have succeeded in employing the same mathematical formalism for both spectra and angular distributions, the method of Ref. 12 also yields the exact solution of Eq. (14) in explicit form:

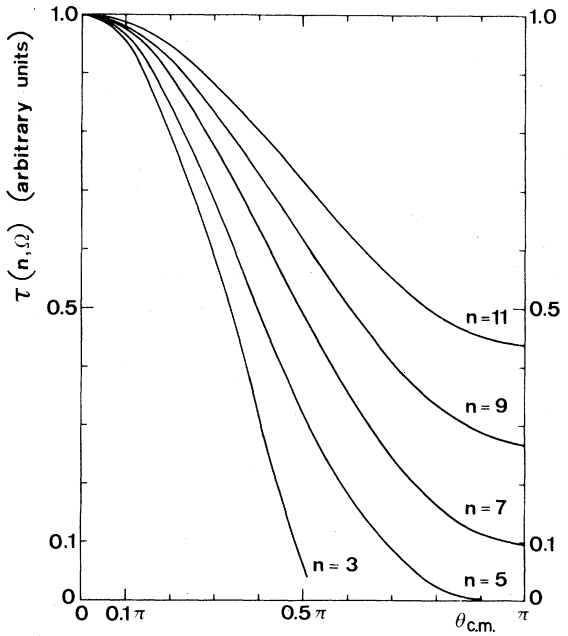

FIG. 3. Angular dependence of mean lifetime $\tau(n,\Omega)$ as calculated from closed-form expression (17), i.e., by neglecting both λ^0 and λ^- transitions. See further, caption of Fig. 2.

$$\zeta_l(n) = \eta_l(n_0, t=0)(\mu_l)^{(n-n_0)/2} T_l(n) h_l(n) \left(\prod_{\substack{m=n_0 \\ \Delta m=2}}^{n-2} \lambda^+(m) T_l(m) h_l(m) \right)$$

$$\times \left\{ 1 + \sum_{\substack{s=n+2 \\ \Delta s=2}}^{N} \left[\prod_{\substack{k=n \\ \Delta k=2}}^{s-2} \mu_l^2 \lambda^+(k) T_l(k) h_l(k) \lambda^-(k+2) T_l(k+2) h_l(k+2) \right] \right\}, \quad (18)$$

where N is the maximum exciton number and

$$T_l(n) = [\lambda^+(n) + \lambda^-(n) + w(n) + (1-\mu_l)\lambda^0(n)]^{-1}, \quad (19a)$$

$$h_l(n) = [1 - \mu_l^2 \lambda^+(n-2) T_l(n-2) \lambda^-(n) T_l(n) h_l(n-2)]^{-1}, \quad (19b)$$

while $h_l(n_0) = 1$. In Eq. (18) the first product within parentheses, clearly representing a depletion factor, should be replaced for $n = n_0$ by a factor one, and the summation has to be set equal to zero for $n = N$. This summation keeps track of the many possible paths, due to the inclusion of both λ^0 and λ^- transitions, for the system to reach the nth exciton state.

In addition, a simple and fast computation method can be given in order to solve Eq. (14). This algorithm holds for an arbitrary initial condition, which may be of interest also to the analysis of gamma-ray or multiparticle emission. First we compute

$$\zeta_l^{(0)}(n_0) = \eta_l(n_0, t=0), \quad (20a)$$

$$\zeta_l^{(0)}(n) = \eta_l(n, t=0) + \mu_l \lambda^+(n-2) T_l(n-2) \times h_l(n-2) \zeta_l^{(0)}(n-2) \quad (n = n_0+2, \ldots, N) \quad (20b)$$

and the solution of Eq. (14) is then given by

$$\zeta_l(N) = T_l(N) h_l(N) \zeta_l^{(0)}(N), \quad (21a)$$

$$\zeta_l(n) = T_l(n) h_l(n) [\zeta_l^{(0)}(n) + \mu_l \lambda^-(n+2) \zeta_l(n+2)] \quad (n = N-2, \ldots, n_0). \quad (21b)$$

Therefore we believe that in solving the (generalized) master equation it is not necessary to make use of simplifying approximations, such as the "never come back" assumption.

III. MODEL SPECIFICATION

Up to now, the discussion has been general. In writing the generalized master equation (2), the angular state Ω of the composite nucleus has been assumed to be identical with the direction of the projectile. Otherwise stated, the influence of the recoil nucleons, which are much slower in most cases, has been neglected. For an extensive discussion of these problems, see Mantzouranis *et al.*[2,3] The only restriction needed to obtain the results of the present paper is that the kernel G depends on the angle α between the considered directions Ω and Ω' alone: $G(\Omega, \Omega') = G(\cos\alpha)$, which is a quite natural condition. With regard to practical applications, one should assume a definite form for this kernel and, in addition, specify an initial condition.

A. Eigenvalues

Following Ref. 3, we suppose the scattering kernel G to be given according to Eq. (1). At the energies of incident particles in most preequilibrium reactions, the free differential nucleon-nucleon cross section $d\sigma^f/d\Omega$ is nearly isotropic in the center-of-mass system of the two nucleons. Assuming isotropy, we may write for the integral kernel G with Ω and Ω' expressed in the center-of-mass system of projectile and target

$$G(\Omega, \Omega') = \pi^{-1} \cos(\theta_{1ab}) H(\pi/2 - \theta_{1ab}) \frac{d\Omega_{1ab}}{d\Omega}, \quad (22)$$

where H is the Heaviside function and θ_{1ab} is the angle between the directions Ω_{1ab} and Ω'_{1ab} in the laboratory frame. (Note that we are dealing with three different reference systems. First, we deal with the nucleon-nucleon c.m. system, in which the nucleon-nucleon cross section is assumed to be isotropic. Second, we consider the laboratory frame, indicated by the index "lab." Third, we have the c.m. system of projectile and target; in this system the quantities are not indexed. The Jacobian $d\Omega_{1ab}/d\Omega$ is introduced in order to transform all relevant quantities to the latter system.)

The expression for the eigenvalues now becomes, according to Eqs. (6) and (22),

$$\mu_l = 2 \int_{-\beta}^{1} \frac{(x+\beta)(1+\beta x)}{(1+2\beta x+\beta^2)^2} P_l(x) dx, \quad (23)$$

where β stands for the ratio of the masses of the projectile and the target nucleus. Due to the fact that preequilibrium theory deals mostly with heavy nuclei and light incident particles, in many cases it is a good approximation to assume an infinitely heavy target nucleus. Setting β equal to zero in Eq. (23), the integral may be explicitly calculated[13]:

$$\mu_l = \begin{cases} 1 & (l=0), \\ \frac{2}{3} & (l=1), \\ 0 & (l \text{ odd},\ l \neq 1), \\ \dfrac{(-1)^{(l+2)/2}(l!)}{2^{l-1}(l-1)(l+2)[(l/2)!]^2} & (l \text{ even}). \end{cases} \tag{24}$$

If one takes, on the other hand, the limit $\beta \to 1$, Eq. (23) reduces to the assumption of isotropy as introduced in the beginning of this section.

B. Initial condition

We adopt as the initial condition

$$q(n, \Omega, t=0) = \delta_{nn_0} \pi^{-1} \cos(\theta_{1ab}) H(\pi/2 - \theta_{1ab}) \times \frac{d\Omega_{1ab}}{d\Omega}, \tag{25}$$

where θ_{1ab} stands for the angle between the incident direction and Ω_{1ab} in the laboratory system. This condition corresponds to the angular distribution after one collision, according to the assumed isotropy of the nucleon-nucleon scattering cross section. Because of the fact that the initial condition (25) is proportional to the scattering kernel G, the Legendre expansion coefficients $\eta_l(n, t=0)$ of the initial condition can be expressed in terms of the eigenvalues μ_l only. One obtains

$$\eta_l(n, t=0) = \delta_{nn_0}(4\pi)^{-1}(2l+1)\mu_l . \tag{26}$$

For neutron-induced reactions it is most straightforward to use Eq. (25) with $n_0 = 3$ as the initial condition. In doing this, the Pauli principle and several compensating effects of the nuclear geometry are neglected, such as the finite size of the nucleus, refraction of the incident wave, and refraction or reflection of the outgoing wave at the nuclear surface.[3] The geometry effects may be very important at the rather low energies considered in the next part of this paper (Sec. IV). To give a rough estimate for the refraction of the incident particle, in this work we have adopted the quasiclassical approximation in the limit of a large refractive index, being useful at low incident energies. This approximation leads to Eq. (25) with $n_0 = 1$ [in addition we have taken a vanishing value for the emission rate $w(1) = 0$, thus suppressing elastic scattering]. This gives exactly the same angle-integrated emission spectra, but less-forward-peaked angular distributions, in better agreement with experimental data.[14] The other effects mentioned are not separately accounted for; in Sec. IV B the deviations from the model specification given here are empirically investigated by adjusting the kernel G occurring in Eqs. (22) and (25).

Now the model is completely specified. With respect to the angle-integrated exciton model, the only new quantities needed to describe the angular distributions are the characteristic values μ_l [compare Eqs. (3) and (8)]. Keeping in mind that $\underline{B}_0$ is identical with the transition matrix of the standard master equation (3), it is not difficult to show that

$$\int \tau(n, \Omega) d\Omega = \tau(n), \tag{27}$$

where $\tau(n) = \int_0^\infty q(n, t) dt$, the mean lifetime of the nth exciton state. Moreover, the isotropic (zeroth order) part of the time integral $\tau(n, \Omega)$ always equals $(4\pi)^{-1}$ times the angle-integrated time integral $\tau(n)$ of the occupation probability. Accordingly, the above scheme leads to an entirely consistent picture.

Finally, we address the problem of convergence of the Legendre series for $\tau(n, \Omega)$. For simplicity, let us suppose that the eigenvalues μ_l are given according to Eq. (24), i.e., $\beta = 0$ approximation. Applying Stirling's formula, it follows that

$$\tfrac{4}{3} l^{-5/2} \leq |\mu_l| \leq \tfrac{5}{3} l^{-5/2} \quad (l > 2), \tag{28a}$$

and in the limit for high values of l,

$$|\mu_l| \to 2(2/\pi)^{1/2} l^{-5/2}. \tag{28b}$$

Combining Eqs. (28) with the initial condition (26), the absolute convergence for all exciton numbers n is easily checked for all expressions derived for $\tau(n, \Omega)$ in Sec. II. Equations (28) also indicate that the higher-order contributions rapidly decrease with respect to the isotropic part, even for the lower exciton states. This suggests that in many numerical calculations it will be sufficient to consider only a few Legendre polynomials. The numerical calculations carried out, and presented in the next section, confirm the usefulness of the present model at this particular point. It has to be noted, however, that with a truncated Legendre polynomial series, slightly negative values may result for $G(\Omega, \Omega')$ at large angles.

IV. COMPARISON WITH EXPERIMENTAL DATA

A. Experimental data base

The simple mathematical solution of the generalized master equation given in Secs. II and III facilitates the calculation of angular distributions for a large number of cases. An extensive set of angular distributions of inelastically scattered neutrons has been measured at 14.6 MeV by Hermsdorf *et al.*[5] This homogeneous set of data spans a large mass range, thus constituting a

useful data base for a systematical comparison with calculations. Part of the work discussed in this section has been discussed in more detail in a laboratory report.[14]

The data of Hermsdorf *et al.* are neutron emission spectra measured from 2 to 14 MeV at five scattering angles. It should be noted that not only neutrons from the (n,n') reaction, but also neutrons from other processes, mainly from the $(n,2n)$ reaction, contribute to these spectra. Since the $(n,2n)$ reaction gives rise to two emitted neutrons, the spectra have to be interpreted as

$$S(E,\epsilon,\theta)=d^2\sigma_{nn'}/d\epsilon d\Omega+2d^2\sigma_{n\,2n}/d\epsilon d\Omega .$$

These data have been integrated over 1-MeV energy bins between 2 and 11 MeV by the experimenters.

The quantities $S(E,\epsilon,\theta)$ have been used to calculate Legendre coefficients by means of a least-squares fitting procedure. For each value of ϵ three coefficients ($l=0$, 1, and 2) with standard deviations and correlation coefficients were computed. In most cases the normalized values of χ^2 appeared to be much larger than unity; therefore the errors were multiplied with the square root of χ^2. The reason for these rather bad fits originates from the fact that the measured spectra are not smooth functions of ϵ, but display a considerable fine structure.[5] On the other hand, the (statistical) uncertainties in the measurements are quite small. In Fig. 4 the three-term Legendre polynomials fitted to the 1-MeV averaged experimental data for iodine are shown. More examples of these fits are given in Ref. 14.

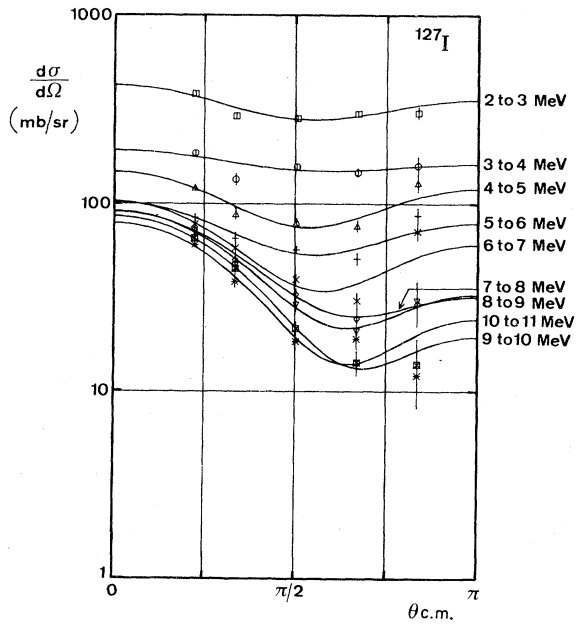

FIG. 4. Experimental angular distributions of neutrons emitted from the reaction ^{127}I+n at $E=14.6$ MeV. The data points have been integrated over 1-MeV intervals by Hermsdorf *et al.* The solid curves represent three-term Legendre polynomials fitted to these data points, expressed in center-of-mass coordinates.

The observed structure in the data suggests that for intercomparisons with statistical-model results, much larger energy intervals must be considered. Therefore, we have summed the Legendre coefficients over the energy ranges from 2 to 11 MeV and from 6 to 11 MeV. In the last-mentioned energy range, competing processes are either absent or give negligible contributions, so that a good comparison with calculated angular distributions of inelastically scattered neutrons is possible. This approach follows that of Pearlstein,[15] who has recently performed a similar intercomparison, but only for angle-integrated data. The experimental data, summed over the range $\Delta\epsilon=6$–11 MeV are given in Table I, where the Legendre coefficients have been normalized according to

$$\frac{d\sigma_{nn'}^{\rm exp}(\Delta\epsilon,\theta)}{d\Omega}=\frac{\sigma_{nn'}^{\rm exp}(\Delta\epsilon)}{4\pi}\left[1+3f_1P_1(\cos\theta)+5f_2P_2(\cos\theta)\right]. \quad (29)$$

In Fig. 5 the thin lines represent the Legendre polynomials fitted to the summed experimental iodine data. It is clear that much of the structure observed in Fig. 4 has disappeared in Fig. 5. Other examples of these fits are given in Figs. 6–11.

B. Calculations with global parameters

The code PREANG (Ref. 7) has been used to compute the emission spectra and angular distributions. The angle-integrated cross sections are calculated in this code according to the paper of Běták,[16] with the improved solution of the master equation as described by Luider.[8] In all calculations it was assumed that the target element consisted of only one, i.e., the most abundant, isotope. For the single-particle level-density parameter g, and the average transition matrix element M^2, the usual global parameters $g=A/13$ and $M^2=190/A^3E$ (Ref. 17) were adopted in our calculations. The pairing-energy corrections P were taken from Gilbert and Cameron.[18] The inverse neutron reaction cross sections were calculated according to the optical model with parameters of Wilmore and Hodgson.[19] Competitive charged-particle reactions were taken into account for protons and α particles, using inverse reaction cross sections calculated from optical models as specified in Refs. 20 and 21, respectively.

TABLE I. Experimental and calculated integrated (n,n') cross sections and angular distribution coefficients in the energy range from 6 to 11 MeV.

Element	$\sigma_{nn'}$ (6–11 MeV) Exp.	$\sigma_{nn'}$ (6–11 MeV) Calc. 1 [a]	f_1 (6–11 MeV) Exp.	f_1 (6–11 MeV) Calc. 1 [a]	f_2 (6–11 MeV) Exp.	f_2 (6–11 MeV) Calc. 1 [a]
Be	211 ± 16	172 [b]	0.21 ± 0.03	0.28 [b]	0.10 ± 0.04	0.017 [b]
C	146 ± 6	182 [b]	0.19 ± 0.02	0.20 [b]	0.14 ± 0.02	0.013 [b]
Na	192 ± 8	266	0.13 ± 0.02	0.25	0.09 ± 0.03	0.028
Mg	181 ± 5	102 [b]	0.25 ± 0.01	0.24 [b]	0.12 ± 0.01	0.023 [b]
Al	167 ± 3	196	0.18 ± 0.01	0.27	0.07 ± 0.01	0.027
Si	141 ± 4	133 [b]	0.16 ± 0.02	0.26 [b]	0.06 ± 0.02	0.027 [b]
P	199 ± 10	199	0.23 ± 0.02	0.27	0.11 ± 0.03	0.028
S	180 ± 13	125	0.32 ± 0.04	0.30	0.03 ± 0.04	0.032
Ca	263 ± 25	100	0.28 ± 0.04	0.32	0.18 ± 0.07	0.036
Ti	183 ± 6	141	0.34 ± 0.02	0.33	0.07 ± 0.02	0.038
V	146 ± 7	211	0.24 ± 0.03	0.33	0.18 ± 0.02	0.037
Cr	212 ± 8	162	0.25 ± 0.02	0.33	0.08 ± 0.02	0.038
Mn	154 ± 9	212	0.19 ± 0.02	0.33	0.09 ± 0.03	0.037
Fe	132 ± 5	162	0.14 ± 0.02	0.34	0.06 ± 0.02	0.040
Co	95 ± 4	207	0.16 ± 0.03	0.33	0.06 ± 0.02	0.038
Ni	114 ± 3	142	0.18 ± 0.01	0.34	0.07 ± 0.02	0.040
Cu	131 ± 7	192	0.09 ± 0.03	0.33	0.12 ± 0.03	0.039
Zn	123 ± 6	159	0.19 ± 0.02	0.35	0.05 ± 0.02	0.041
Ga	206 ± 10	194	0.17 ± 0.03	0.34	0.09 ± 0.03	0.040
Se	233 ± 16	165	0.17 ± 0.04	0.37	0.13 ± 0.04	0.045
Br	193 ± 8	183	0.16 ± 0.02	0.35	0.11 ± 0.02	0.042
Zr	198 ± 21	190	0.17 ± 0.05	0.37	0.10 ± 0.05	0.045
Nb	180 ± 7	227	0.36 ± 0.02	0.36	0.11 ± 0.02	0.042
Cd	185 ± 4	201	0.22 ± 0.01	0.38	0.09 ± 0.01	0.047
In	217 ± 6	218	0.22 ± 0.02	0.37	0.11 ± 0.01	0.045
Sn	236 ± 8	209	0.21 ± 0.02	0.38	0.11 ± 0.02	0.047
Sb	189 ± 16	219	0.32 ± 0.04	0.38	0.07 ± 0.04	0.045
I	247 ± 7	222	0.24 ± 0.02	0.38	0.12 ± 0.02	0.045
Ta	211 ± 17	280	0.38 ± 0.04	0.38	0.10 ± 0.05	0.045
W	301 ± 13	287	0.32 ± 0.02	0.39	0.14 ± 0.02	0.046
Au	239 ± 9	251	0.15 ± 0.02	0.39	0.04 ± 0.02	0.046
Hg	347 ± 29	257	0.31 ± 0.04	0.39	0.18 ± 0.05	0.048
Pb	350 ± 21	386	0.27 ± 0.03	0.38	0.13 ± 0.04	0.045
Bi	356 ± 23	369	0.26 ± 0.03	0.37	0.14 ± 0.04	0.044

[a] Calculation 1: $g=A/13$, P according to Gilbert and Cameron (Ref. 18).

[b] Extrapolations have been used to obtain values at the highest emission energies, where the level densities vanish due to large pairing energy corrections.

Secondary particle emission was not accounted for in the calculations. This means that the calculated neutron cross sections correspond to the spectrum of the first emitted neutron; see also Sec. IV D.

The Legendre coefficients were calculated in the code PREANG as described in Secs. II and III. For the first three expansion coefficients of $G(\Omega,\Omega')$ we have adopted the formulas $\mu_0=1$, $\mu_1=\frac{2}{3}-\beta/2-2\beta^2/15$, and $\mu_2=\frac{1}{4}-4\beta/5+\beta^2/4$, where $\beta=1/A$. These expressions approximate the integral given for μ_l in Eq. (23). Higher-order Legendre coefficients were not calculated because of the fast convergence of the Legendre polynomial series (Sec. III B) and because the experimental data were also analyzed with only three terms. The calculated Legendre coefficients were averaged over 1-MeV intervals and renormalized in the same way as for the experimental coefficients. The calculated quantities summed from 6 to 11 MeV are given in Table I (Calc. 1). It should be noted that for a number of nuclides the results are unreliable due to excessive pairing-energy corrections; see Sec. IV C. For these cases the 1-MeV averaged data at the highest emission energies have been extrapolated by assuming the Legendre coefficients to be constant. The ratios of experimental and calculated values are displayed in Fig. 12, where it has been assumed that the logarithms of the ratios have symmetric errors. The weighted mean values and standard deviations according to the lognormal distribution

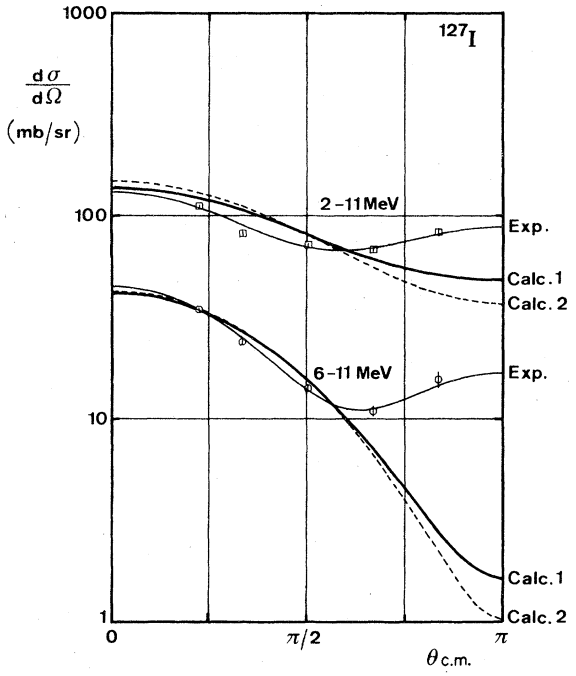

FIG. 5. Experimental and calculated angular distributions of neutrons emitted from the reaction ^{127}I+n at $E=14.6$ MeV. The data have been integrated from $\epsilon=2$–11 MeV and $\epsilon=6$–11 MeV. The curves labeled Exp represent three-term Legendre fits through the experimental data of Hermsdorf *et al.* Calculation 1 was obtained from exciton-model calculations with the usual global parameters. In Calc. 2 the approximated closed-form expression (17) was used at $n<\bar{n}$. In both calculations the angular distributions are seriously underestimated at the backward angles.

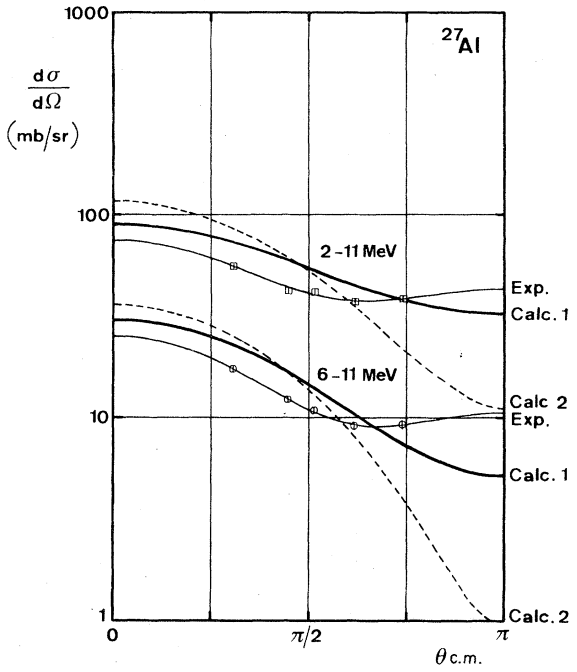

FIG. 6. Experimental and calculated angular distributions of neutrons emitted from the reaction ^{27}Al +n at $E=14.6$ MeV. For explanation of symbols see caption of Fig. 5. This figure illustrates that the approximation of Calc. 2 is less good for light nuclides.

are indicated in Fig. 12 and Table II.

A first conclusion of the results of Calc. 1 with standard parameters is that the mean values of the integral cross section ratios (given in Table II) are very close to unity and that there are no large systematic deviations as a function of the mass number (see Fig. 12). Thus, with a simple set of global parameters it is possible to obtain quite good fits for the angle-integrated cross sections.

The calculated angular distribution coefficients f_1 given in Table I are systematically too high, whereas the f_2 coefficients are much too low. Furthermore, there are some systematical deviations as a function of mass number, in particular, for $A=60$–80; see Fig. 12. Some examples of Calc. 1 are given in Figs. 5, 6, 8, and 10, together with experimental angular distributions and results of other calculations. From these figures it follows that reasonably good agreement is obtained at forward angles, although the angular distribution is underpredicted at the backward

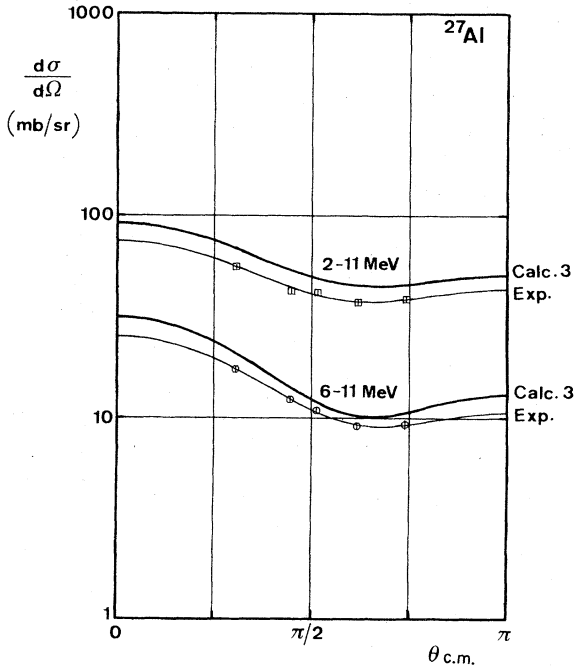

FIG. 7. Experimental and calculated angular distributions of neutrons emitted from the reaction ^{27}Al+n at $E=14.6$ MeV. The curves labeled Calc. 3 were obtained from a calculation with two adjusted global parameters μ_1 and μ_2 to fit the experimental Legendre coefficients for 34 nuclides. Note the improvements at backward angles, compared with Calc. 1 (Fig. 6).

angles. For some other elements, e.g., Fe, the agreement between experimental data and the results of Calc. 1 is less satisfactory, also at the forward angles; see further Sec. IV C.

Before trying to improve the angular distribution results by means of adjustment of global model parameters, we discuss the results of Calc. 2 (see Table II), in which the simple closed-form expression given in Eq. (17) was used to calculate the angular distributions. This expression was derived by assuming that $\Delta n = 0$ and $\Delta n = -2$ transitions are not possible. We have substituted Eq. (17) into our code, assuming isotropy for particles emitted from exciton states with $n \geq \bar{n}$. Using the same mean lifetimes $\tau(n)$ and the same input parameters as in Calc. 1, we obtained much more forward-peaked angular distributions for nuclides with mass numbers below $A \approx 90$. In fact, f_1 (6–11 MeV) varied only from 0.37 to 0.40 over the entire mass range. This shows that, in particular, for nuclides with light masses the $\Delta n = 0$ and $\Delta n = -2$ transitions have to be taken into account. Apparently these transitions are more important for nuclides with light mass numbers, where $\bar{n}$ is not much higher than n_0 at the energies considered here. This conclusion may be of importance for hybrid-model calculations.[22] In Figs.

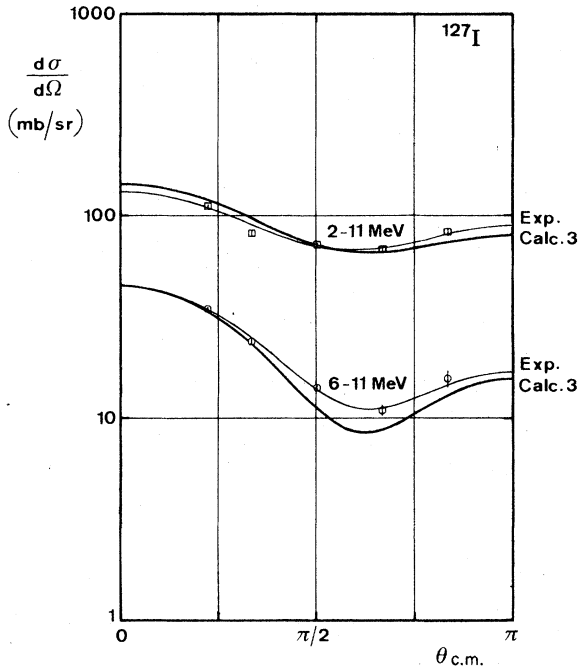

FIG. 9. Experimental and calculated angular distributions of neutrons emitted from the reaction ^{127}I+ n at $E = 14.6$ MeV. Calculation 3 gives much better results at backward angles, compared with Calc. 1 (Fig. 5). See captions of previous figures for explanation of symbols.

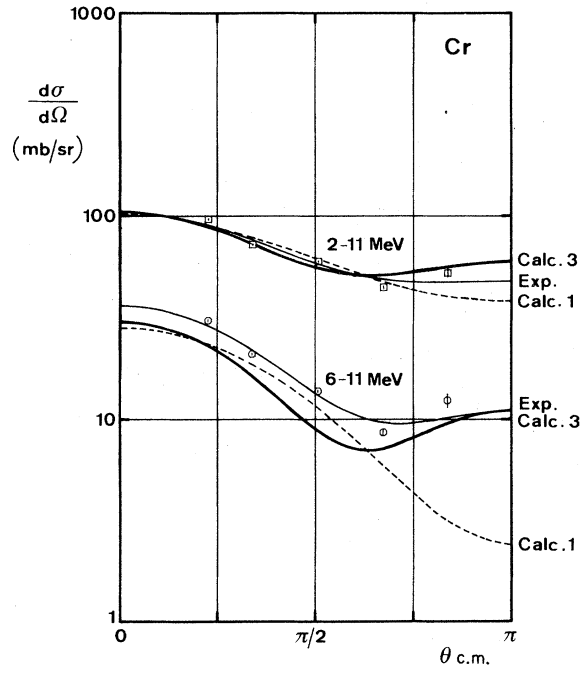

FIG. 8. Experimental and calculated angular distributions of neutrons emitted from the reaction Cr+n at $E = 14.6$ MeV. Calculation 3 gives much better results at backward angles, compared with Calc. 1. See captions of previous figures for explanation of symbols.

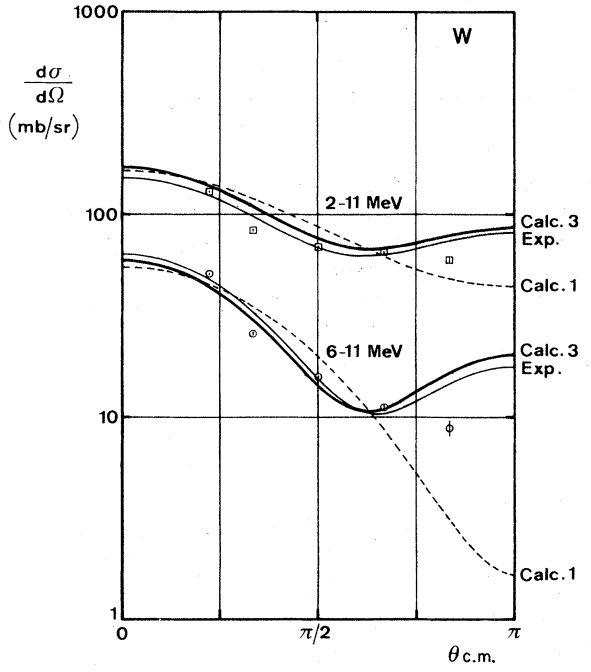

FIG. 10. Experimental and calculated angular distributions of neutrons emitted from the reaction W+n at $E = 14.6$ MeV. Calculation 3 gives much better results at backward angles, compared with Calc. 1. See captions of previous figures for explanation of symbols.

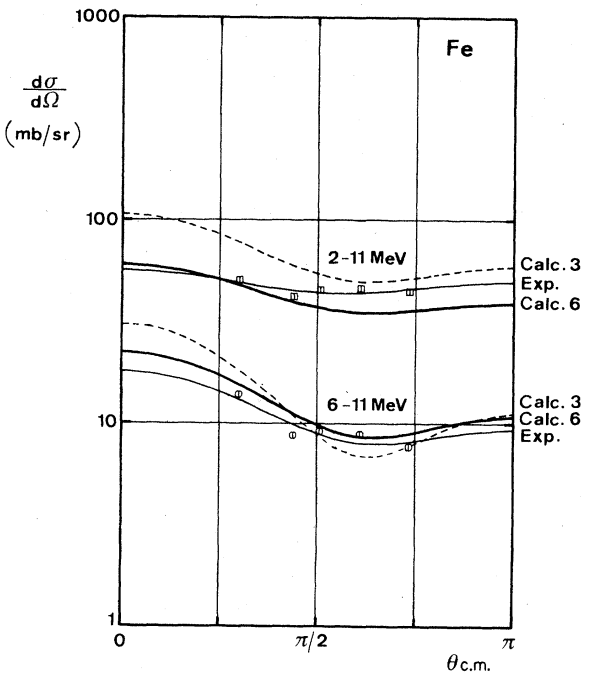

FIG. 11. Experimental and calculated angular distributions of neutrons emitted from the reaction Fe + n at $E = 14.6$ MeV. This curve illustrates that adjustment of level-density parameters of ^{56}Fe (Calc. 6) gives further improvements, compared with Calcs. 1 and and 3. This applies particularly for nuclides in the mass range $A = 60$–80 and to magic nuclides. See captions of previous figures for explanation of symbols.

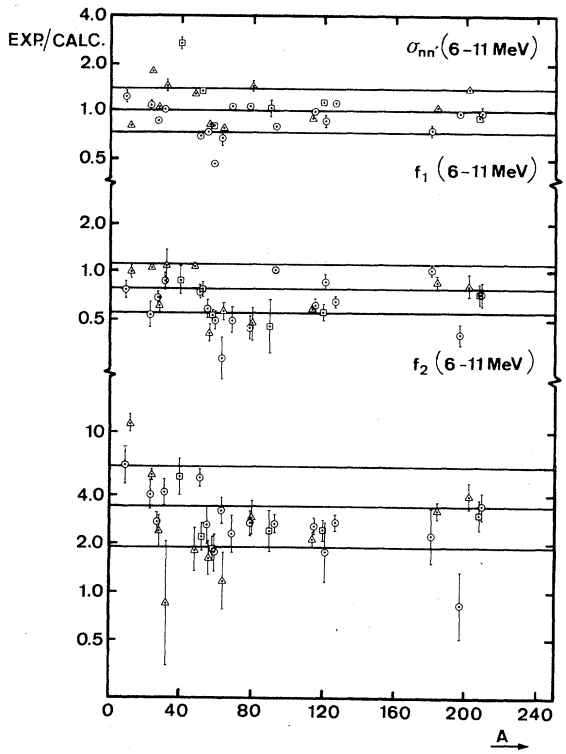

FIG. 12. Ratio of experimental and calculated Legendre coefficients of neutron emission cross sections of neutron-induced reactions at 14.6 MeV as a function of the target mass number. The experimental coefficients [see Eq. (29)] were obtained from three-term Legendre polynomial fits to experimental data of Hermsdorf *et al.*, integrated from $\epsilon = 6$–11 MeV. The calculated coefficients were obtained from Calc. 1, with standard exciton-model parameters. Circles, triangles, and squares stand for odd A, even A, and magic N or Z, respectively. The average values and standard deviations are indicated by horizontal lines. See also Tables I and II (Calc. 1).

5 and 6 the results of Calc. 2 are compared with those of Calc. 1 for I and Al, respectively.

Returning to the discussion of results of Calc. 1, we note that all calculations seem to underpredict the values of f_2, which mainly affects the cross sections at backward scattering angles. In fact, the model parameters specified in Sec. III always led to decreasing cross sections as a function of angle. However, from the experimental data it follows that quite often the cross sections increase at backward angles. An empirical way of improving these results could be to modify the adopted angular distribution of the kernel $G(\Omega, \Omega')$ by adjusting its Legendre coefficients. We found that multiplication factors of μ_1 and μ_2 of 0.87 and 1.74, respectively, were needed to obtain a minimum value of χ^2 for the coefficients f_1 and f_2 (see Table II, Calc. 3). Some results of Calc. 3 are also shown in Figs. 7–11; similar figures for all 34 nuclides are given in Ref. 14. Quite acceptable fits were obtained for most nuclides with these two global parameters. This is completely in line with the present status of preequilibrium theory, where effective parameters such as $g = A/13$ and $M^2 = 190/A^3E$ are currently used. It is difficult to give a quantitative physical explanation for the proposed adjusted parameters, μ_1 and μ_2. It is likely that they result from geometry effects not explicitly included in the model (see Sec. III B). We notice, however, that the adjusted global parameters are mass independent, in contrast to the empirical formula proposed in Ref. 3 to account for finite-size effects. Also, these global parameters might partly be the result of the limited validity, in particular at lower energies, of the "fast-particle" concept (compare Fig. 2 of Ref. 3). Remaining discrepancies are mainly found in mass regions where the nucleon numbers are magic or nearly magic. Therefore, besides further improvement of the angular distribution theory itself, it is necessary to devote some attention to the level-density problem.

TABLE II. Overall comparison of experimental and calculated data for 34 nuclides.

Calc.[a] No.	ΔE (MeV)	Exp./Calc. cross section	χ^2	Exp./Calc. f_1 coeff.	χ^2	Exp./Calc. f_2 coeff.	χ^2
1	2–11	0.95[b]	66	0.52[b]	14	3.6[b]	7.0
1	6–11	$0.98^{+0.36}_{-0.26}$[c]	26	$0.76^{+0.33}_{-0.23}$[c]	10	$3.2^{+2.5}_{-1.4}$[c]	4.6
2	2–11	See Calc. 1		0.34[b]	36	2.7[b]	6.0
2	6–11			$0.63^{+0.26}_{-0.18}$[c]	19	$2.5^{+1.5}_{-0.95}$[c]	3.8
3	2–11	See Calc. 1		0.72[b]	7.5	1.10[b]	5.0
3	6–11			$1.03^{+0.45}_{-0.31}$[c]	5.0	$1.00^{+0.78}_{-0.44}$[c]	2.9
4	2–11	1.00[b]	102	0.68[b]	22	4.8[b]	7.3
4	6–11	$1.2^{+1.1}_{-0.6}$[c]	76	$0.82^{+0.41}_{-0.27}$[c]	10	$3.5^{+3.2}_{-1.7}$[c]	4.8
5	2–11	0.92[b]	60	0.74[b]	5.5	5.4[b]	7.8
5	6–11	$0.87^{+0.24}_{-0.19}$[c]	32	$0.97^{+0.27}_{-0.21}$[c]	3.6	$4.1^{+3.1}_{-1.8}$[c]	5.3
6	2–11	See Calc. 5		See Calc. 5		1.3[b]	4.8
6	6–11					$1.0^{+0.77}_{-0.44}$[c]	2.8

[a] Calculation 1: standard exciton model parameters, $g = A/13$, P according to Ref. 18.
Calculation 2: approximated closed-form expression, Eq. (17).
Calculation 3: adjusted μ_1 and μ_2 values, multiplication factors of 0.87 and 1.74, respectively.
Calculation 4: level-density parameters with shell corrections according to Ref. 18.
Calculation 5: adjusted final-state level densities (Table III) without pairing-energy corrections.
Calculation 6: as Calc. 5, with adjusted μ_2, multiplication factor of 1.95.
[b] Arithmetic mean value.
[c] Weighted mean values and standard deviations according to lognormal distribution.

C. Variation of level-density parameters

In the adopted model the particle-hole density formula of Ericson[23] with some additional corrections introduced by Williams[24] and Běták[25] have been used. This formula contains only two parameters, the single-particle level-density parameter g, usually taken as $A/13$, and the pairing-energy shift P. Evidently, this gives a rather poor description of the experimental level density over a large mass and energy range. Therefore, the sensitivity of the calculated results to the adopted level-density parameters was investigated.

In a first attempt to improve the results of Calc. 1 we have modified g according to $g = (6/\pi^2)(0.00917S + 0.142)A$, where the shell corrections S were taken from Gilbert and Cameron.[18] This modification gave far less satisfactory results for the angle-integrated cross sections, notably for nuclides with closed or nearly closed shells, such as those near Pb (Ref. 14). The overall results of this calculation are given in Table II, Calc. 4. Quite remarkably, the results for f_1 and f_2 were almost the same, even for the magic nuclides.[14]

In order to understand these results, we have investigated the role of the level densities of the compound and residual nuclides g_c and g_r, respectively. It appears that a decrease of g_c leads to enhanced preequilibrium components in the spectra and thus enhancement of f_1. This follows from the fact that g_c, like M^2, enters into the expression for the internal transition rates. A decrease of g_r reduces f_1, but may give rise to either enhancement or reduction of the high-energy tail of the spectra, because apart from the reduction of preequilibrium emission, the spectrum shape is flattened.

The use of more realistic values for g_c would also imply a change in the previously fitted values of $M^2 = 190/A^3E$ (Ref. 17), as both parameters enter the expressions for the internal transition rates. Since in fact, the main task of g_c is to control these transition rates, it was decided to keep g_c at its usual value $A/13$. In further calculations we have only varied the values of g_r and P_r.

The adopted level density, summed over all possible particle and hole numbers, is in good agreement with the expression for a one-fermion gas[26]:

$$\rho(E) = \frac{1}{\sqrt{48}} \exp(2\sqrt{aU})/U \quad (E \gg P), \tag{30}$$

where $a = (\pi^2/6)\, g$ and $U = E - P$. Evidently, this formula only holds at energies much larger than the pairing-energy correction, although it is still used at energies very close to P. This leads to the underprediction of the high-energy tails of the energy spectra, mentioned before. Therefore, in the usual statistical model, other—more empirical—formulas[18,27] are employed, the parameters of which have been fitted to obtain agreement with experimental information from low-lying states and neutron resonances. The simplest of these approaches is the "back-shifted" Fermi-gas model,[27] where only two parameters are adjusted, a and Δ. The last-mentioned parameter appeared to be negative for many nuclides, in contrast to Eq. (30), where the (positive) pairing energy P causes a forward shift. Although there is a large discrepancy between forward- and backward-shifted level-density formulas, both descriptions are used in statistical-model calculations. It is very important to overcome these problems in connection with the preequilibrium model, at least at the fairly low excitation energies considered in this paper. A more fundamental treatment of the level-density problem is highly desired. A simple starting point of such an investigation could be the renormalization of particle-hole densities such that the summed level density agrees with the back-shifted Fermi-gas model.

Meanwhile, a practical way of studying at least some effects of level-density parameters of the residual nuclides on spectra and angular distributions could be to drop P_r, while adjusting g_r. From calculations with various values for g_r, it turned out that it was possible to obtain good agreement for both the angle-integrated spectra and the f_1 coefficients, with standard deviations of less than 30% and a rather good representation of the experimentally observed mass dependence of f_1; see Tables II and III (Calc. 5) and further intercomparisons in Ref. 14. Moreover, in a number of cases the calculated energy dependence of the spectra and f_1 coefficients was considerably improved, particularly for the lighter elements.[14] Although these results are not based upon realistic level densities, they show very clearly the importance of level-density parameters in the calculations.

A further improvement of the results of Calc. 5 was obtained by multiplying μ_2 with 1.95, in order to fit the experimental f_2 values; see Table II, Calc. 6. In Fig. 11 the results have been plotted for Fe, together with those of Calc. 3. Similar good fits were obtained for most other elements in the mass range $A = 60$–80. Impressive improvements were also obtained for Ca (Ref. 14).

TABLE III. Experimental and calculated f_1 coefficients in the energy range from 6 to 11 MeV with adjusted level densities.

Element	f_1 (6–11 MeV) Exp.	f_1 (6–11 MeV) Calcs. 5, 6 [a]	Adjusted g [a] (MeV^{-1})
Be	0.21 ± 0.03	0.23	0.41
C	0.19 ± 0.02	0.29	0.76
Na	0.13 ± 0.02	0.13	1.02
Mg	0.25 ± 0.01	0.22	1.20
Al	0.18 ± 0.01	0.18	1.46
Si	0.16 ± 0.02	0.14	1.01
P	0.23 ± 0.02	0.21	1.86
S	0.32 ± 0.04	0.27	1.99
Ca	0.28 ± 0.04	0.29	2.50
Ti	0.34 ± 0.02	0.29	2.97
V	0.24 ± 0.03	0.20	2.53
Cr	0.25 ± 0.02	0.28	3.07
Mn	0.19 ± 0.02	0.19	2.67
Fe	0.14 ± 0.02	0.16	1.87
Co	0.16 ± 0.03	0.19	2.88
Ni	0.18 ± 0.01	0.17	2.25
Cu	0.09 ± 0.03	0.13	2.54
Zn	0.19 ± 0.02	0.18	2.47
Ga	0.17 ± 0.03	0.19	3.21
Se	0.17 ± 0.04	0.31	4.49
Br	0.16 ± 0.02	0.14	3.14
Zr	0.17 ± 0.05	0.15	3.15
Nb	0.36 ± 0.02	0.32	5.50
Cd	0.22 ± 0.01	0.26	5.00
In	0.22 ± 0.02	0.30	6.00
Sn	0.21 ± 0.02	0.25	5.00
Sb	0.32 ± 0.04	0.33	6.79
I	0.24 ± 0.02	0.34	7.44
Ta	0.38 ± 0.04	0.38	11.7
W	0.32 ± 0.02	0.37	12.4
Au	0.15 ± 0.02	0.38	12.5
Hg	0.31 ± 0.04	0.38	14.0
Pb	0.27 ± 0.03	0.37	14.2
Bi	0.26 ± 0.03	0.37	15.1

[a] Compound-nucleus level densities as in Calc. 1; adjusted final-state level densities without pairing-energy corrections.

D. Relation with Hauser-Feshbach model

There are many differences between Hauser-Feshbach (HF) type of calculations and exciton-model calculations. In the exciton model, the description of the reaction process is more general, but angular momentum effects, excitation of discrete levels, and multiparticle emission are not taken into account, whereas the adopted level-density formulas are not very realistic (Sec. IV C). The relation between the HF, exciton, and various direct reaction models is not well established at present. We assume that direct single-particle transitions are included in the exciton model in a statistical way, but that direct collective excitations are not accounted for. In this section neutron emission spectra calculated with rigorously

applied HF theory are compared with those calculated with the exciton model. It is shown that when the exciton model is used to simulate equilibrium emission, there is good agreement between the results of both calculations, provided that the same level-density parameters are used. This fact offers the possibility to connect the two models in a consistent way.

The simulation of pure equilibrium emission in the framework of the exciton model was performed by looking for the stationary solution of the angle-integrated master equation (3):

$$\frac{dq(n)}{dt}=0\,. \tag{31}$$

Detailed balance (and, of course, neglect of emission) leads to the condition

$$q(n)=q(n-2)\lambda^{+}(n-2)/\lambda^{-}(n)\,. \tag{32}$$

Thus, a proper definition of the equilibrium exciton distribution is obtained by the relations

$$q(n)=q(n_0)\prod_{\substack{m=n_0+2\\ \Delta m=2}}^{n}\lambda^{+}(m-2)/\lambda^{-}(m)\,,$$
$$\sum_n q(n)=1\,. \tag{33}$$

By considering $q(n)$ as the initial exciton distribution [instead of $q(n)=\delta_{nn_0}$], the angle-integrated and time-integrated master equation is easily solved,[12] yielding the equilibrium emission.

The HF calculations were performed with the recently developed code PENELOPE,[6] which was used to calculate emission spectra of the reactions $(n,n'\gamma)$, $(n,2n)$, (n,np), $(n,n\alpha)$, (n,pn), $(n,\alpha n)$, and $(n,\gamma n)$ for ^{93}Nb and ^{127}I targets. These calculations were performed with carefully evaluated optical-model parameters, level-scheme data, and level-density parameters. For the decription of the level density, a slightly modified version[28] of the composite Gilbert-Cameron formula[18] was used, the parameters of which were obtained from fits to recent level schemes and neutron resonances or from systematics.[28] Some results are shown in Figs. 13 and 14, with indication of the major components of the emission spectra. At emission energies below about 6 MeV, the predominant components come from the $(n,2n)$ reaction, from which the first and second neutron emission spectra are plotted separately in Fig. 13, It should be noted that the sum of these two contributions needs to be added to the other contributions to compare with the angle-integrated and energy-averaged data of Hermsdorf *et al.* On the other hand, for a comparison with coincidence measurements of Schröder *et al.*,[29] performed for the reaction ^{127}I$(n,2n)^{126}$I at $E=14.1$ MeV, the average of the two $(n,2n)$ spectra is required; see Fig. 14. Both figures show that $(n,2n)$ contributions are reasonably well described with the HF model. This suggests that, at not too high energies, the HF model can be successfully used, if a preequilibrium calculation is introduced for the emission of the first neutron only.

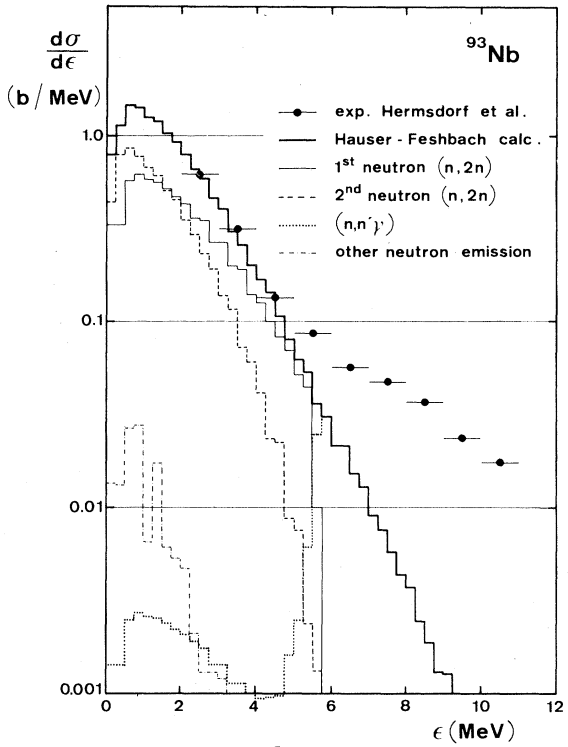

FIG. 13. Experimental and calculated neutron emission spectra of the reaction ^{93}Nb+n at 14.6 MeV. The experimental data of Hermsdorf *et al.* have been integrated over $\Delta\epsilon=1$ MeV and $\Delta\Omega=4\pi$. All calculations have been performed with the HF code PENELOPE, without any parameter adjustment. The figure shows the calculated total neutron emission spectrum with various components, integrated over 0.25-MeV intervals. Below $\epsilon=5.77$ MeV the $(n,2n)$ reaction dominates; at higher emission energies there is only inelastic scattering. Fluctuations in the calculated curves are due to excitation of discrete levels or to threshold effects. In particular, in the (n,pn) and $(n,\alpha n)$ reactions, discrete levels are excited by neutrons with rather small energies. The results at $\epsilon<0.5$ MeV are not very accurate in this calculation. The figure illustrates the complexity of the shapes of the neutron spectrum components at low emission energies, which at present can only be calculated with sophisticated HF models. There is good agreement with experimental data for energies below 5 MeV.

As has been discussed before, our present exciton model does not take into account multiparticle emission. For the sake of comparison, we have added the HF emission spectra of the

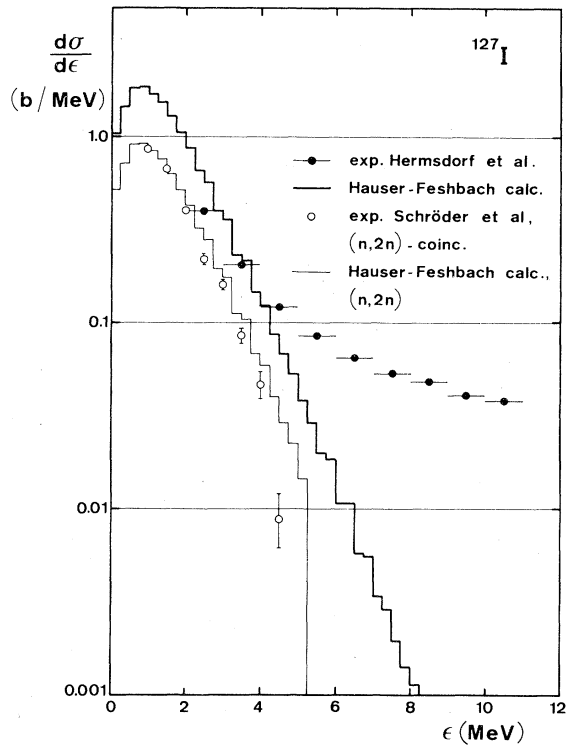

FIG. 14. Experimental and calculated neutron emission spectra of the reaction ^{93}Nb+n at E=14.6 MeV. The experimental data are neutron spectrum measurements of Hermsdorf *et al.* and $(n,2n)$ coincidence measurements of Schröder *et al.* (at 14.1 MeV). The calculations have been performed with the HF code PENELOPE, without any parameter adjustment. Shown are the calculated total emission spectrum and the $(n,2n)$ spectrum, obtained by averaging the neutron spectra for the first- and second-emitted neutrons. The figure illustrates the capacity of the HF model in calculations of emission spectra at low energies.

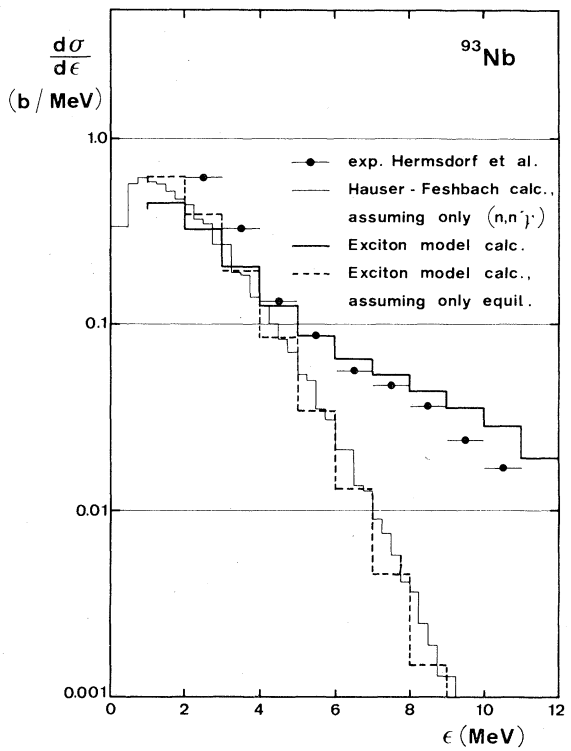

FIG. 15. Results of exciton-model and HF calculations assuming no secondary particle emission in the emission spectrum of the ^{93}Nb(n,n') reaction. The dashed curve was obtained by assuming that the initial exciton distribution was at equilibrium, Eq. (23). This figure illustrates the consistency between the HF model and exciton model. It also shows the failure of the HF model at high emission energies, where the measurements correspond to inelastic scattering only.

$(n, n'\gamma)$, (n,np), and $(n,n\alpha)$ reactions and of the first-emitted neutron in the $(n,2n)$ reaction. The resulting HF spectrum may be compared with the equilibrium spectrum calculated from the exciton model. As follows from Fig. 15, the results of this intercomparison are quite satisfactory. The adopted level-density parameters for ^{93}Nb were almost the same in both calculations, i.e., a=11.65 and 11.76 MeV^{-1} in the HF and exciton-model calculations, respectively. With this proviso, the two models are seen to be consistent (compare the conclusions of Cline and Blann[4]). Therefore, energy distributions calculated with the HF model for those channels where preequilibrium effects are important, could very well be replaced by energy distributions calculated with the adopted exciton model. A similar remark applies to the calculation of angular distributions.

Instead of trying to include preequilibrium effects in HF type of calculations, an alternative approach could be to refine the present exciton model by including multiparticle emission (e.g., Ref. 30), angular momentum effects, γ-ray emission (e.g., Ref. 31), and discrete level excitation.

V. CONCLUSIONS

Our formulation of the generalized exciton model leads to an extremely simple description. Special characteristics are the following:

1. The same mathematical formalism applies to the analysis of both energy and angular distributions.
2. The Legendre coefficients of the angular distributions are directly calculated.
3. A unified description (at least in principle) of preequilibrium and equilibrium stages of the reaction is followed.
4. Transitions with $\Delta n = 0$ explicitly influence the shape of the angular distributions, in contrast to the angle-integrated spectra.
5. Mean lifetimes and their Legendre coeffi-

cients can be calculated with a fast, explicit formula [Eq. (18) or Eqs. (20) and (21)], without the introduction of approximations.

The mathematical improvements to the generalized exciton model presented in this paper greatly facilitate a systematical comparison with experimental data. The calculations performed for neutron emission spectra, measured at incoming neutron energy of 14.6 MeV, indicate that the adopted model describes energy distributions better than angular distributions which appear to be systematically underestimated at the backward angles. Still, the generalized exciton model is reported[32] to be more useful in this respect than the alternative intranuclear cascade model. We have shown that the approximation of the "never come back" assumption, occurring in the hybrid model and in some formulations of the exciton model, leads to further underestimation of the angular distribution at backward angles for the light nuclides ($A < 90$). An encouraging result, in favor of the generalized exciton model, is that a good overall fit of the angular distributions for all 34 nuclides was obtained by adjustment of only two global parameters, which empirically account for several physical phenomena in the nucleus not explicitly included in the model (Sec. IV B). Though quantitative physical arguments for this adjustment are lacking at present, this would imply that a good description of angular distributions for a very large mass range can be obtained with the aid of a few global parameters only, as in the case of the angle-integrated spectra. Therefore, the generalized exciton model is promising, but further theoretical effort is needed. It seems that, particularly, the assumptions made in the specification of the model (Sec. III) are too drastic. We also conclude that the results are very sensitive to the choice made for the initial condition of the angular distribution. This is to be expected because the shape of the angular distribution is largely determined by emission from the lowest exciton states. Therefore, further improvement of the expression for the initial condition, Eq. (25), is very important. By assuming $n_0 = 1$ [and $w(1) = 0$] for nucleon-induced reactions, a rough estimate has been given for the effect of refraction of the incident particle at the nuclear surface. This leads to improved agreement with measured data at 14.6 MeV.

The extension of the model to angular distributions opens up new possibilities for improving preequilibrium theory as a whole. It appears that in several respects the nuclear level densities are not properly treated in the exciton model, at least at the fairly low excitation energies considered in this paper (Sec. IV C). From various calculations with different values of the final-state level-density parameters it was found that the agreement between experimental and calculated data could be improved for the first-order Legendre coefficient of the angular distribution (f_1) as well as for the angle-integrated spectra (Tables I and III). Therefore, it seems that much of the observed structure in f_1 (Table I) should be ascribed to level-density effects. A critical reexamination of the level-density problem is highly desirable. Another important problem is the unification of the statistical Hauser-Feshbach model and the exciton model. Although our adopted exciton model includes equilibrium emission, its description of the deexcitation of the compound state is rather crude compared with rigorously applied HF theory. However, a proper definition of equilibrium emission in the framework of the exciton model leads to very similar emission spectra as is shown in Sec. IV D. This consistency allows the introduction of preequilibrium effects in the HF model. Alternatively, the exciton model could be refined by including multiparticle emission, angular momentum effects, etc. We expect that the simplicity of the present description of the generalized exciton model will greatly facilitate these model extensions.

ACKNOWLEDGMENT

We thank Mr. B. P. J. van den Bos for his great help in the exciton-model calculations.

*Present address: FOM-Institute for Plasma Physics, Rijnhuizen, P. O. Box 7, 3430 AA Nieuwegein, The Netherlands.

[1]J. M. Akkermans, Phys. Lett. 82B, 20 (1979).
[2]G. Mantzouranis, D. Agassi, and H. A. Weidenmüller, Phys. Lett. 57B, 220 (1975).
[3]G. Mantzouranis, H. A. Weidenmüller, and D. Agassi, Z. Phys. A276, 145 (1976).
[4]C. K. Cline and M. Blann, Nucl. Phys. A172, 225 (1971).
[5]D. Hermsdorf *et al.*, Zentralinstitut für Kernforschung, Rossendorf bei Dresden Report No. ZfK-277 (1974).
[6]G. Reffo (unpublished).
[7]J. M. Akkermans and H. Gruppelaar, Netherlands En-

ergy Research Foundation Report No. ECN-60 (1979).
[8]F. J. Luider, Z. Phys. A284, 187 (1978).
[9]F. R. Gantmacher, *Matrix Theory* (Chelsea, New York, 1960), Vol. II, pp. 53–62.
[10]E. Gadioli, E. Gadioli Erba, L. Sajo Bohus, and G. Tagliaferri, Riv. Nuovo Cimento 6, 1 (1976).
[11]M. Blann, Annu. Rev. Nucl. Sci. 25, 123 (1975).
[12]J. M. Akkermans, Z. Phys. A292, 57 (1979).
[13]I. M. Ryshik and I. S. Gradstein, *Tables of Series, Products and Integrals*, 2nd ed. (VEB Deutscher Verlag der Wissenschaften, Berlin, 1964), p. 244.
[14]H. Gruppelaar and J. M. Akkermans, Netherlands Energy Research Foundation, ECN report (unpublished).
[15]S. Pearlstein, Nucl. Sci. Eng. 68, 55 (1978).
[16]E. Běták, Comp. Phys. Comm. 9, 92 (1975); 10, 71 (1975).
[17]C. Kalbach-Cline, Nucl. Phys. A120, 590 (1973).
[18]A. Gilbert and A. G. W. Cameron, Can. J. Phys. 43, 1446 (1965).
[19]D. Wilmore and P. E. Hodgson, Nucl. Phys. 55, 673 (1964).
[20]F. Perey and B. Buck, Nucl. Phys. 32, 353 (1962).
[21]G. Igo and J. R. Huizenga, Nucl. Phys. 29, 462 (1962).
[22]G. Mantzouranis, Phys. Lett. 63B, 25 (1976).
[23]T. Ericson, Adv. Phys. 9, 425 (1960).
[24]F. C. Williams, Nucl. Phys. A166, 231 (1971).
[25]E. Běták and J. Dobeš, Z. Phys. A279, 319 (1976).
[26]C. van Lier and G. E. Uhlenbeck, Physica 4, 531 (1937).
[27]W. Dilg, W. Schantl, and H. Vonach, Nucl. Phys. A217, 269 (1973).
[28]G. Reffo, Comitato Nazionale Energia Nucleare, Bologna, Report No. RT/FI(78)11 (1978).
[29]V. Schröder, W. Scobel, L. Wilde, and M. Bormann, Z. Phys. A287, 353 (1978).
[30]V. S. Ol'khovskiĭ and V. A. Plyuĭko, Yad. Fiz. 25, 520 (1977) [Sov. J. Nucl. Phys. 25, 279 (1977)].
[31]E. Běták and J. Dobeš, Phys. Lett. 84B, 368 (1976).
[32]G. Mantzouranis, Phys. Rev. C 14, 2018 (1976).